EUROPEAN FUSION DEVELOPMENT AGREEMENT

EFDA–JET–CP(04)07-27

D.C. McDonald, J. G. Cordey, K-D. Zastrow, I. Voitsekhovitch, C.C. Petty, M. de Baar, E. Joffrin, E. de la Luna, P. de Vries, G. Maddison, P.J. Lomas, J. Snipes, J. Stober, D. Stork and JET EFDA Contributors

Particle and Energy Transport in Dedicated ρ*, β and ν* Scans in JET ELMy H-modes

Particle and Energy Transport in Dedicated ρ*, β and ν* Scans in JET ELMy H-modes

D.C. McDonald[1], J. G. Cordey[1], K-D. Zastrow[1], I. Voitsekhovitch[1], C.C. Petty[2], M. de Baar[3], E. Joffrin[4], E. de la Luna[5], P. de Vries[1], G. Maddison[1], P.J. Lomas[1], J. Snipes[6], J. Stober[7], D. Stork[1] and JET EFDA Contributors*

[1]EURATOM/UKAEA Fusion Association, Culham Science Centre, Abingdon Oxon OX14 3DB, UK
[2]General Atomics, P. O. Box 85608, San Diego, CA 92186-5608, USA
[3]FOM-Rijhuizen, Ass. Euratom-FOM, TEC, P. O. Box 1207, 3430 BE Nieuwegein, NL
[4]Association Euratom-CEA, CEA Cadarache, F-13108, St. Paul lez Durance, France
[5]Laboratorio Nacional de Fusion, Asociacion EURATOM-CIEMAT, Madrid, Spain
[6]Massachusetts Institute of Technology, Cambridge, MA 02139, USA
[7]Max Planck-Institute fur Plasmaphysik, EURATOM Association, D-85748 Garching, Germany
** See annex of J. Pamela et al, "Overview of JET Results ", (Proc.20 [th] IAEA Fusion Energy Conference, Vilamoura, Portugal (2004).*

Preprint of Paper to be submitted for publication in Proceedings of the
20th IAEA Conference,
(Vilamoura, Portugal 1-6 November 2004)

ABSTRACT.

Studying plasma transport in terms of the non-dimensional parameters ($\rho*$,β, $\nu*$) is a natural way to separate important physical transport processes. $\rho*$, the ion Larmor radius normalised to the plasma minor radius, separates Bohm/gyro-Bohm transport; β, the ratio of plasma pressure to magnetic pressure separates electrostatic and electromagnetic transport; and $\nu*$, the ion collision rate scaled to the ion bounce frequency, describes the effect of collisionality. With this in mind, scans have been performed on JET (Mark IIGB-SRP divertor) with one of $\rho*$, β, $\nu*$ varied whilst the other two remained fixed. Both particle transport, using trace tritium (T) injection, and energy transport have been studied. The $\rho*$ behaviour of energy and trace T transport is found to be consistent with the essentially gyro-Bohm like dependence of the scaling used in the ITER design, IPB98(y,2), although trace T confinement in the outer region (x = 0.65-0.85) is Bohm like ($D/B_0 \propto \rho^{*-1.90\pm0.38}$). The $\nu*$ scans showed energy confinement decreasing with increasing $\nu*$ ($B_0.\tau_E \propto \nu^{*-0.35\pm0.04}$) more strongly than in IPB98(y,2), with trace T confinement having the opposite trend although the results are more ambiguous. In contrast to IPB98(y,2) the three β scans show a negligible effect of β on energy confinement ($B_0.\tau_E \propto \beta^{*0.04}$, $\beta^{*-0.03}$, $\beta^{*-0.01}$), which is consistent with electrostatic models. Trace T confinement, however, increases with increasing β ($D \mu D_{g\text{-}Bohm}.\beta^{*-0.34\pm0.08}$, $D \propto D_{Bohm}.\beta^{*-0.55\pm0.09}$) which is inconsistent with IPB98(y,2) and electrostatic models, but is shown to be consistent with a model based on stochastic electromagnetic fields. It remains to describe both particle and energy transport with a unified model. Extrapolation of these results to ITER indicates a moderate increase in energy confinement time for $\beta_N = 1.8$ (2%), but a dramatic improvement for higher β_N (e.g. 50% higher for $\beta_N = 3$). The impact on ITER of increased particle confinement at high β_N remains to be assessed.

1. INTRODUCTION

In the ITER design [1], energy and particle confinement are based upon IPB98(y,2) scalings,

$$\tau_E = \tau_{IPB98(y,2)} = 5.62 \times 10^{-2} \times P_{loss}^{-0.69} B_0^{0.15} I_p^{0.93} \kappa_a^{0.78} \bar{n}_e^{0.41} a^{0.58} R^{1.39} M^{0.19} \qquad (1a)$$

$$\tau_{p,He} = 5 \times \tau_{IPB98(y,2)}, \qquad (1b)$$

which have been derived from a wide database (DB3v5) of multi-machine confinement experiments [2] and, in the case of energy confinement, are consistent with experimental measures over almost 3 orders of magnitude. The IPB98(y,2) scaling has been shown to be consistent with the Kadomtsev [3] constraint, and so may be cast in the dimensionless form

$$B_0 \tau_{IPB98(y,2)} \propto \rho^{*-2.70} \beta^{-0.90} \nu^{*-0.01} M^{0.96} q_{95}^{-3.0} \varepsilon^{0.73} \kappa^{3.3} \qquad (2)$$

Dimensionless variable scans on a single machine involve a series of discharges at different fields.

In each type of scan, one dimensionless variable varies whilst the rest are fixed. This implies that plasma current, density and temperature must all vary as a certain function of the field (Table I). Experimentally, this is achieved through the direct selection of plasma current and the tuning of gas fuelling and input power until variables are matched within their measurement errors (taken for JET as 2.7% for ρ^*, 6.0% for β, 10.4% for ν^*, and 8.3% for $B\tau_E$ [4]). A bulk ion particle transport ρ^* scan experiment has been performed previously at JET [5], indicating a mixture of Bohm and gyro-Bohm transport, but the other parameters were not well matched. Dimensionless parameter scan studies of energy transport have been performed on several machines, including JET [6], but the ones presented here are more extensive.

Table I: scaling of VARIABLES in dimensionless parameter scans

Scanned parameter	Fixed parameters	Scalings
$\boldsymbol{\rho^*} \propto T^{1/2}/B_0$	β, ν^*, q_{95}	$I \propto B_0$, $n \propto B_0^{4/3}$, $T \propto B_0^{2/3}$
$\boldsymbol{\beta} \propto nT/B_0^2$	ρ^*, ν^*, q_{95}	$I \propto B_0$, $n \propto B_0^4$, $T \propto B_0^2$
$\boldsymbol{\nu^*} \propto n/T^2$	ρ^*, β, q_{95}	$I \propto B_0$, $n \propto B_0^0$, $T \propto B_0^2$

2. PARTICLE TRANSPORT EXPERIMENTS WITH TRACE TRITIUM

Table II: Discharges for trace tritium ELMy H-mode (ρ^*, β, ν^*) scans

Pulse	Time (s)	I_p (MA)	ρ^*/ρ^*_{ITER}	β_N	ν^*/ν^*_{ITER}	D_{inner}/B_0 ($m^2s^{-1}T^{-1}$)	D_{outer}/B_0 ($m^2s^{-1}T^{-1}$)
61103	14.0	2.75	2.46	1.68	1.90	0.137	0.277
61174	22.0	2.35	2.84	1.89	2.03	0.280	0.364
61097	23.0	2.00	3.14	1.88	2.34	0.291	0.440
61132	23.0	2.35	2.77	0.58	1.53	0.137	0.393
61530	22.0	2.00	2.88	1.94	3.63	0.151	0.260

Bulk particle transport has been studied by monitoring the propagation of trace tritium (T) using 14 MeV neutron cameras with 10 horizontal and 9 vertical channels (see [7] for a fuller discussion). To provide the dimensionless variable scans, ELMy H-mode discharges, at low q (q_{95} = 2.8) and triangularity (δ = 0.2), were prepared in pure deuterium plasmas as outlined in section 1. In each case, these were then repeated with a trace T gas puff (2.5-5 mg over 80ms). In all but one case (the mid-ρ^* point), a matched discharge was also performed with T seeding from a 100keV NBI source (1.2MW for 100ms) to separate out wall fuelling effects. The resulting discharges (Table II) provided a three-point ρ^* scan (Pulse No's: 61103, 61174 and 61097), a two-point β scan (Pulse No's: 61103

and61132), and a two-point ν* scan (Pulse No's: 61174 and61530). The low β discharge in the β scan is a Type III ELMy H-mode and problems of access to the Type III regime led to the relatively poor match in ρ* and ν*.

Particle transport of the tritons is described by an advection, v, and diffusion, D, model

$$\frac{\delta n_T}{\delta t} = \nabla \cdot (n_T v - D \nabla n_T) + s. \qquad (3)$$

The edge source was measured by visible spectroscopy and the source profile, s, was calculated from it using a neutral particle model. Assuming v and D to be functions of the bulk species, they can be taken as constant in time. They are then parameterised (3 parameters for D and 3 for v) and the T density profile as a function of time is forward modelled and the 14MeV neutron data resulting from it calculated. D and v are then varied until the closest least squares fit to the neutron data is found. This is performed by the UTC code with the transport modelling performed by the 1Ω-D impurity transport model SANCO and the resulting 14MeV neutrons calculated by a method based on the TRANSP code (see [7] for a fuller discussion). This paper will concentrate on the diffusion coefficient, which is parameterised to have constant values in the regions x = 0-0.45, x = 0.65-0.85 and x = 0.86-1.0, and to be linearly connected in between (x is defined as the square root of the toroidal flux normalised to its value at the separatrix). Figure1 shows the resulting fits to two discharges (Pulse No's: 61097 and 61103) and figure 2 the calculated diffusion profile for discharge Pulse No: 61097. Transport will be studied in the inner (x = 0-0.45) and outer (x = 0.65-0.85) regions, as the region from x = 0.85-1.0 is assumed to be affected by ELMs.

The two discharges in figure 1 represent the high and low points in the ρ* scan and it can be seen that the time for the T puff to penetrate to the core in the high ρ* discharge (Pulse No: 61097) is considerably shorter than that for the low ρ* (Pulse No: 61103) discharge. This can be interpreted as an increase in diffusivity (Fig.3), D_T, with increasing ρ*. A log-linear regression to the inner and outer diffusion measures gives the scalings

$$D_{inner} / B_0 \propto \rho^{*3.22-0.62}, \qquad D_{outer} / B_0 \propto \rho^{*1.90-0.38}. \qquad (4)$$

A strong, gyro-Bohm like, dependence is seen in the inner region and a weaker, Bohm like, dependence in the outer region, both with relatively large standard deviations. Proceeding in a similar vein for the β and ν* scans, gives

$$\begin{aligned} D_{inner} / D_{g\text{-}Bohm} &\; \beta^{-0.34-0.08}, & D_{outer} / D_{Bohm} &\; \beta^{-0.55-0.09}, \\ D_{inner} / B_0 &\propto \nu^{*-0.51-0.17}, & D_{outer} / B_0 &\propto \nu^{*00.40-0.15}, \end{aligned} \qquad (5)$$

where, as the match for ρ* in the β scan is relatively poor, the ρ* dependence has been normalised for using the observed gyro-Bohm like and Bohm like scalings.

To test the robustness of the scalings, a further 4 trace T NBI heated ELMy H-mode discharges, with varying configurations and q-profile, were added to the dedicated scans to produce a database of 9 discharges. A log-linear regression of the parameters ($\rho*$, β, $\nu*$,q) to the normalised diffusivity in the region x=0.65-0.85 for this database (Fig.4) gives

$$D_{ELMy} / B_0 \propto \rho^{*0.24} \beta^{-1.06} \nu^{*-0.13} q^{1.81} . \quad (6)$$

As with the dedicated scans, trace T confinement is between Bohm like and gyro-Bohm like, increasing strongly with increasing β and weakly with increasing ν*. In contrast to (1b), the correlation between thermal and trace T diffusivity in the 9 discharges is weak (D/χ=0.3-1.5).

3. ENERGY TRANSPORT EXPERIMENTS

For the energy transport experiments a ν* scan was performed [8] in a high triangularity, high q scenario (q_{95} = 4.4, $\delta \sim 0.4$, κ = 1.7, a=0.92m, R = 2.9m). Plasma current was varied from 0.68-1.17 MA, and B_0 varied from 0.96-1.6T. A set of 4 shots was produced (Fig.5) with a log-linear regression giving an energy confinement scaling of $B_0\tau_E \propto \nu^{*-0.35\pm0.04}$ (RMSE = 6%).

The ρ* scans were performed, in the scenario described in section 2, for both Type I (β_t = 2.6%, I_p = 2-4MA) and Type III (β_t = 1.3%, I_p = 1.3-4.3MA) ELMy H-modes [8]. For the Type III ELMy H-mode scan (Fig.6), a log-linear regression gives an energy confinement scaling of $B_0\tau_E \propto \rho^{*-2.9\pm0.5}$. The Type I ELMy H-mode scan was affected by variations in the power deposition profile. The relatively low NBI penetration for the low ρ* (high density) discharges meant that heating profiles varied considerably across the scan (Fig.7). The resulting ion temperature profiles also varied in broadness (Fig.8), indicating non-stiff profiles in the parameter range explored. The discharges are thus analysed in terms of their local transport. Figure 9 shows the variation in effective thermal diffusivity, $\chi = (n_e \chi_e + n_i \chi_i)/(n_e + n_i)$ with ρ*. A log-linear regression gives $\chi / B_0\tau_E \propto \rho^{*3.2\pm0.4}$.

Two, two-point β scans were also performed, in the same scenario as section 2, along with a three-point β scan in a higher q (q_{95} = 3.2) and triangularity (δ = 0.3) scenario [4]. In contrast to the IPB98(y,2) scaling, only a very weak β dependence is found ($B_0\tau_E \propto \beta^{*0.04}$, $\beta^{*-0.03}$, $\beta^{*-0.01}$ respectively), consistent with transport dominated by electrostatic processes and in agreement with previous dedicated scans [6, 9]. The three-point scan indicates that this effect is not due to a correlation between β and ELM Type. An analysis of the local transport, using the TRANSP code, shows a similar weak dependence of the effective thermal diffusivity across the plasma (Fig. 10). Similar results have been observed in DIII-D [10].

DISCUSSION

The exponents on (ρ*, β, ν*) derived from the experiments of sections 2 and 3 are summarised in Table III. The ρ* scans show that both trace T and energy transport has a largely gyro-Bohm like behaviour. In the outer region, however, trace T confinement shows a Bohm like behaviour in line

with the analysis of earlier JET experiments [5]. The ρ* scans for energy transport were performed in Type I and Type III ELMy H-mode plasmas, with the Type I scan found to be significantly affected by the variation in heating profile across the scan. The resulting variation in temperature profile indicates that the plasmas were in a region of non-stiff transport. It should be noted that $L_T = T/\nabla T$ was in excess of 7cm in all cases. Trace T confinement is found to have a positive dependence on β with an even stronger positive dependence seen in the wider fit. A similar impact of β on trace helium confinement has been observed at DII-D [10]. The effect of β on energy confinement is found to be negligible in all three dedicated scans, even when the scan was solely within Type I ELMs. The local core energy transport is also found to be β independent. In the two point ν* scan, trace T transport is found to be moderately positively dependent on ν*, although the wider fit indicates a weaker dependence. In the energy transport experiment, energy confinement was seen to decrease weakly with increasing ν*.

Table III: Summary of exponents of scalings for the (ρ, β, ν*) scans*

	$IPB_{98(y,2)}$	**Energy**		**Trace T**	
	$B_0\tau_E$	$B_0\tau_E$	χ/B_0	D/B_0	
			x = 0.5	x = 0 - 0.4	x = 0.65 - 0.85
ρ*	−2.7	−2.9–0.5	3.2–0.4	3.22–0.62	1.90–0.38
β	−2.7	0.04–0.22, −0.03–0.16, −0.01–0.11, (3 scans)		−0.34–0.08	−0.55–0.09
ν*	−2.7	−0.35–0.04		−0.51–0.17	−0.40–0.15

For energy transport, the essentially gyro-Bohm like dependence of IPB98(y,2) is thus well verified by the JET ρ* scans in both Type I and Type III ELMy H-modes. The negligible ν* dependence of IPB98(y,2) is contradicted somewhat by the dedicated scan, however, where a moderate negative effect was observed. More extremely, the strongly negative β scaling of IPB98(y,2) has been contradicted by all dedicated β scans, which all show an almost negligible β dependence. Applying the IPB98(y,2) scaling to trace T transport, it can be seen that its ρ* scaling is broadly in agreement with the dedicated scan and the wider fit, but with some evidence of a weaker Bohm-like behaviour in the outer (x = 0.65-0.85) region. The dedicated ν* scan indicates a somewhat stronger and positive effect on trace T confinement, although this was not born out by the wider fit. The β dependence of both the dedicated scan and the wider fit, however, shows a moderate to strong positive effect of β on trace T confinement in contrast to both IPB98(y,2) and the dedicate energy transport β scans. The observation that $D/\chi = 0.3\text{-}1.5$, contradicts a single particle-energy transport scaling, as in (1b).

Electrostatic models, such as the MMM (Fig.11), are not consistent with the observed β dependence of trace T confinement, but a model based on neoclassical particle orbits in stochastic

electromagnetic fields [11] has been shown to be consistent (Fig.11). However, as the dimensionless scans have demonstrated a weak to negligible β scaling for energy transport, it may be postulated that the energy channel is dominated by electrostatic transport. The energy confinement scaling law derived from the ITPA multi-machine database, may be made consistent with this by performing a log-linear regression with both the Kadomtsev and electrostatic constraint imposed. The resulting fit to DB3v5 is

$$\tau_{ES} = 4.87 \times 10^{-2} \, P_{loss}^{-0.55} \, B_0^{0.09} \, I_p^{0.72} \, \kappa_a^{0.74} \, \bar{n}_e^{0.51} \, a^{0.78} \, R^{1.36} \, M^{0.10}, \qquad (7)$$

which has the dimensionless form $B_0\tau_{ES} \propto \rho^{*-2.8} \beta^{0.0} \nu^{*-0.09}$. This has a close to gyro-Bohm scaling, in agreement with the ρ* scans of section 3, but a weaker ν* dependence than for the dedicated ν* scan (N.B. several alternate scalings [10, 4, 8, 12] show a similar weak or negligible β dependence). When applied to the ITER, $\beta_N = 1.8$, Q = 10 baseline point [1] the electrostatic scaling predicts a slightly higher energy confinement time, $\tau_{ES} = 3.75$s, than IPB98(y,2), $\tau_{IPB98(y,2)} = 3.67$s. At higher values of β_N, however, the electrostatic prediction becomes significantly higher than that of IPB98(y,2) (e.g. 50% higher for $\beta_N = 3.0$). The impact of this on ITER operation can be seen by comparing the plots of the ITER density and temperature operational space calculated with the IPB98(y,2) scaling (Fig.12(a)) and with the electrostatic scaling (Fig.12(b)). Both scalings predict Q≥10 for the $\beta_N = 1.8$, $n/n_{GDL} = 0.85$ point. However, for the IPB98(y,2) prediction, Q falls with an increase in β_N at constant density and an increase in density to the Greenwald limit produces little increase in Q. By contrast, for the electrostatic scaling Q can be made to increase to Q = 15 by increasing β_N above 1.8 and an even larger increase in Q can be achieved by increasing density. The trace T experiments indicate an associated unfavourable increase in particle confinement, and the effect of this on helium ash removal remains to be assessed.

ACKNOWLEDGEMENTS

This work was performed under the European Fusion Development Agreement, and funded partly by the UK Engineering and Physical Sciences Council and by Euratom. The authors thank John Mandrekas for supplying the code for producing the POPCON plots.

REFERENCES

[1]. Aymar A, *et al.*, Plasma Phys. Cont. Fusion **44** (2002) 519
[2]. ITER Physics Basis, Nuc. Fus. **39** (1999) 2175
[3]. Kadomtsev B. B., Sov. J. Plasma Phys. **1** (1975) 295
[4]. McDonald D. C., *et al.*, Plasma Phys. Cont. Fusion **46** (2004) A215
[5]. Zastrow K-D. for the JET Team, Nuc. Fusion **39** (1999) 1891
[6]. Christiansen J. P. and Cordey J. G., Nuc. Fus. **38** (1998) 1757
[7]. Zastrow K-D., *et al.*, "*Tritium Transport Experiments on the JET Tokamak*", to appear in Plasma Phys. Cont. Fusion

[8]. Cordey J. G., *et al.*, "The Scaling of Energy Confinement in JET ELMy H-modes with the Dimensionless Physics Parameters", to appear in proceedings of 31st EPS Conf. on Controlled Fusion and Plasma Physics (London, 2004)

[9]. Petty C. C., *et al.*, Nuc. Fus. **38** (1998) 1183

[10]. Petty C. C., *et al.*, Phys. Plasmas **11** (2004) 2514

[11]. Voitsekhovitch I., *et al.*, '*Trace Tritium transport in H-mode JET plasma with different density*', In preparation for Phys. Plasmas

[12]. Cordey J. G., for the ITPA H-Mode Database Working Group, "*The scaling of confinement in ITER with β and collisionality*", this conference

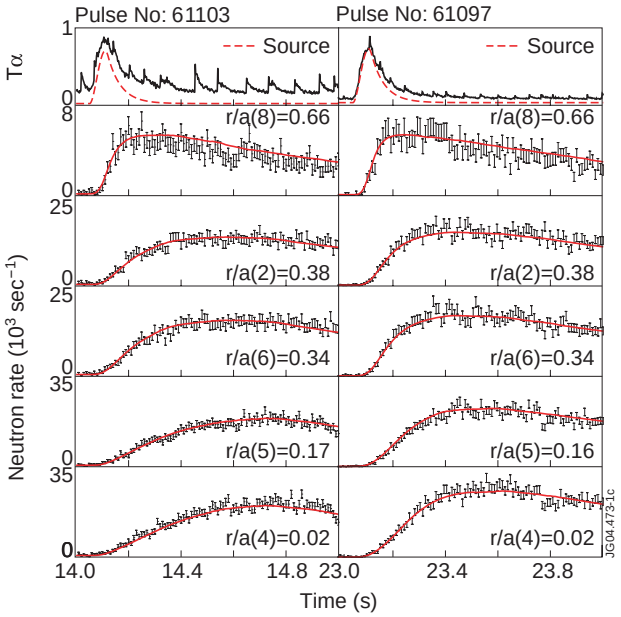

Figure 1: Evolution of the edge T_α (top) and D-T neutron emission, viewed on five different chords (below), following an 80ms T puff, for two Type I ELMy H-Mode shots. Data is shown in black and the prediction from the fitted transport coefficients in pink and red.

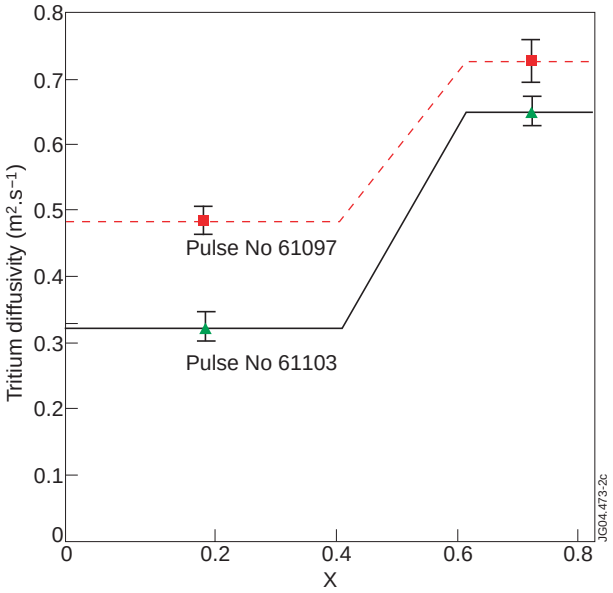

Figurge 2: The T diffusivity profiles for the fits shown in figure 1.

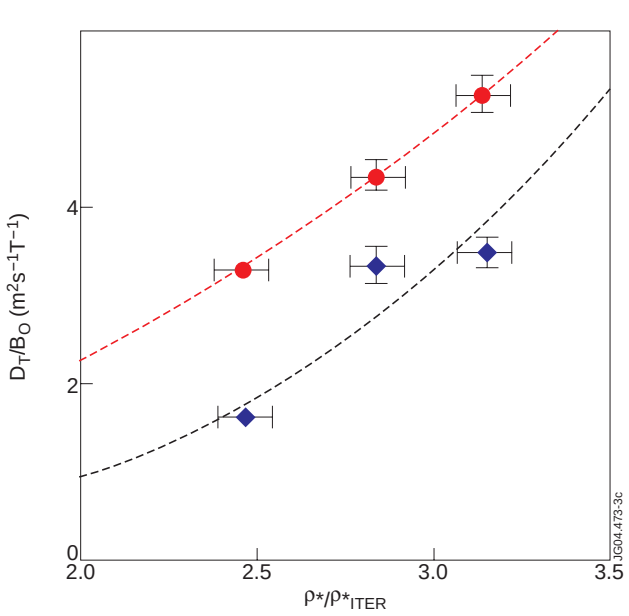

Figurge 3: Normalised T diffusivity, against ρ, normalised to ITER, for the inner (x = 0-0.45; blue diamonds) and outer (x = 0.65-0.85; red circles) regions for Pulse No's: 61103, 61174, and 61097 (Table I). The fits of equation 4 are shown as broken lines.*

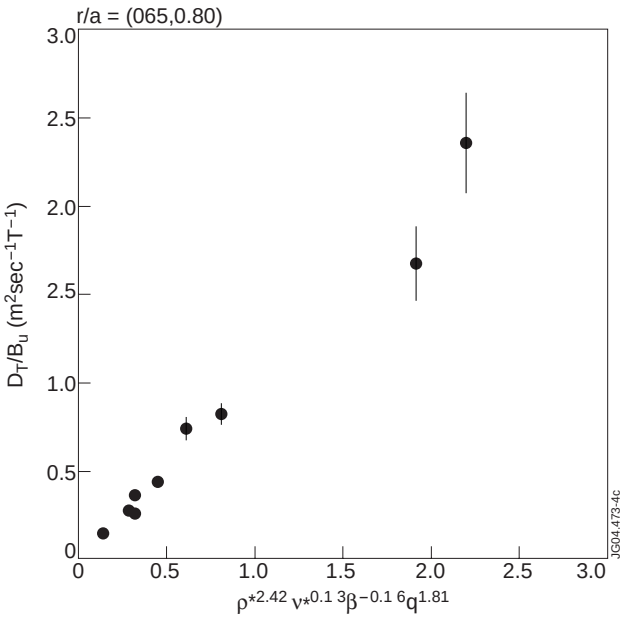

Figurge 4: The normalised diffusivity (x = 0.65-0.85), measured by trace T gas puffing, for 12 ELMy H-modes, against a log-linear regression to the variables (ρ, β, ν*, q) (6)*

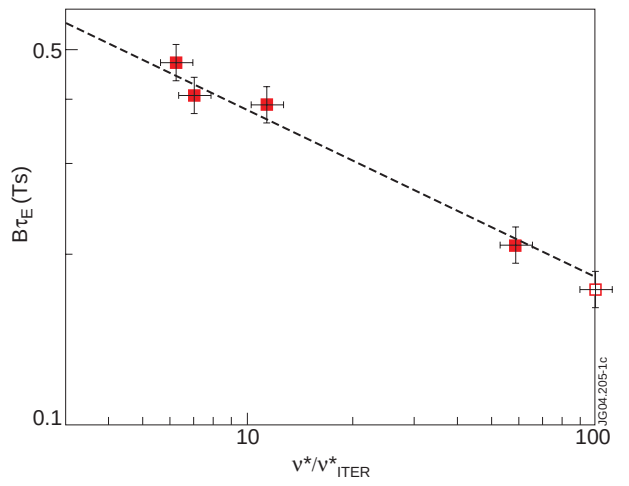

Figurge 5: The normalised confinement time versus the dimensionless collisionality…ν normalised to that in ITER. The best fit (dashed line) is* $B\tau_E \propto \nu^{*\,-0.35}$

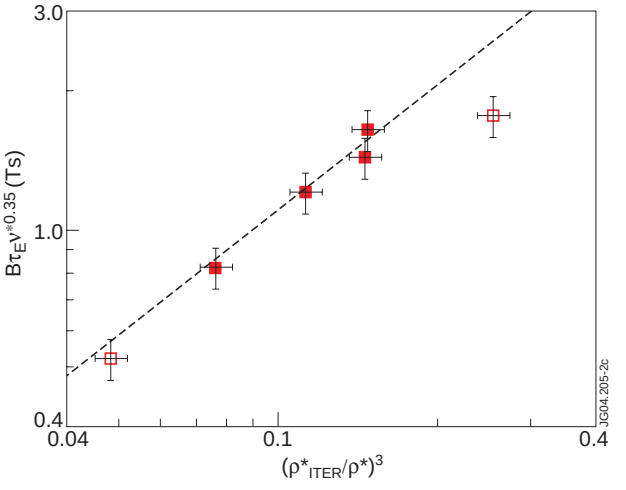

Figurge 6: The normalised confinement time multiplied by $\nu^{*0.35}$ *versus the inverse dimensionless Larmor radius cubed normalised to ITER, for type III ELMy H-modes. The best fit is* $B\tau_E\ \nu^{*0.35} \propto \rho,^{-2.9}$.

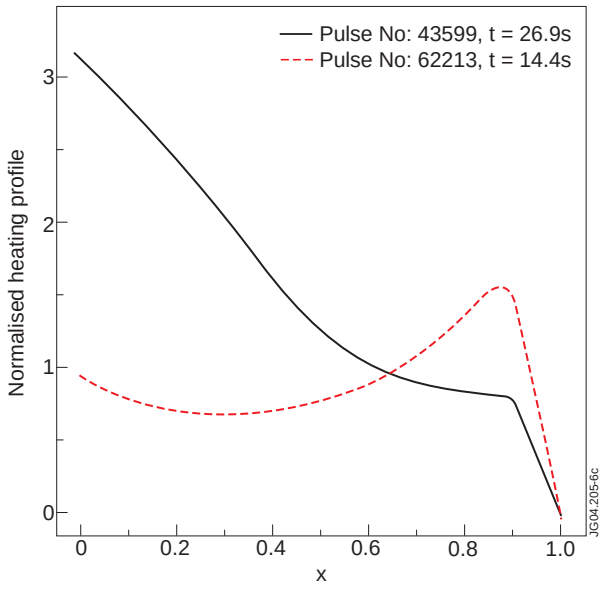

Figurge 7: The heating profiles for the low current (1.46MA) Pulse No's: 43599 and the high current (4MA) 62213.

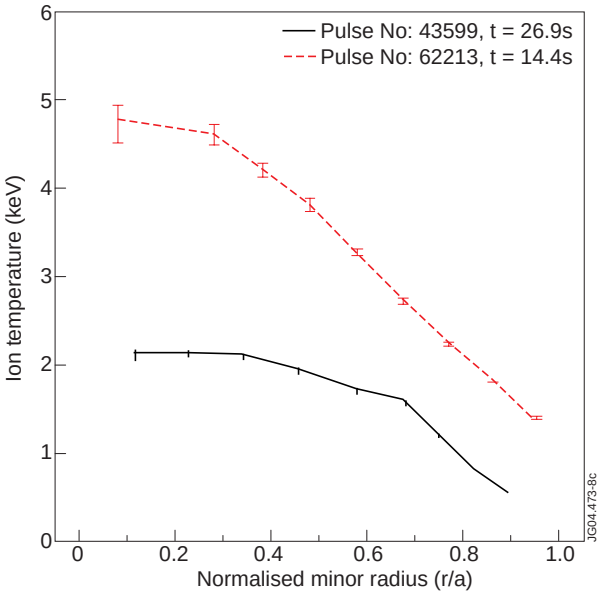

Figurge 8: Ion temperature profiles for the discharges of figure 7.

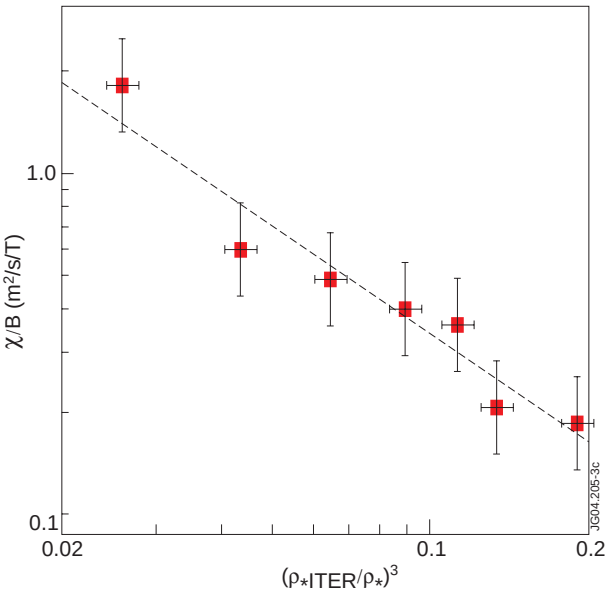

Figure 9: The dimensionless thermal diffusivity χ/B_0 at x = 0.5 versus the inverse global dimensionless Larmor radius cubed normalised to the ITER value. The best fit (dashed line) is $\chi/B_0 \propto \rho^{*3.2}$.

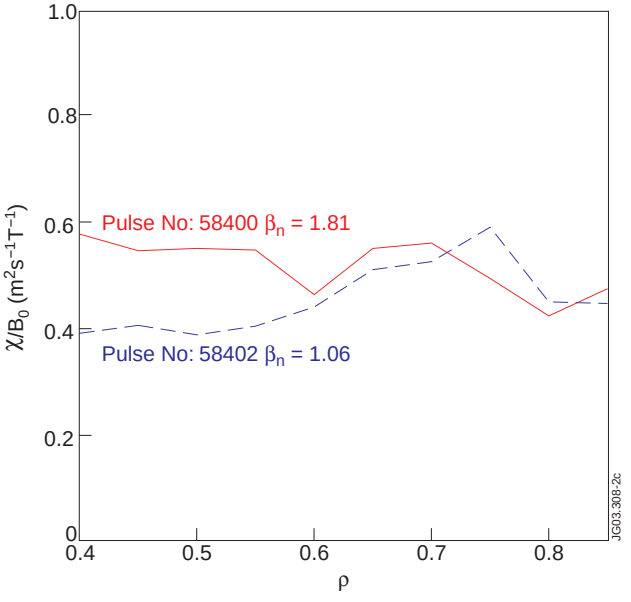

Figure 10: Radial profiles of the effective thermal diffusivity for two ELMy H-mode discharges with matched ρ, ν*, q_{95}, shape and divertor configuration*

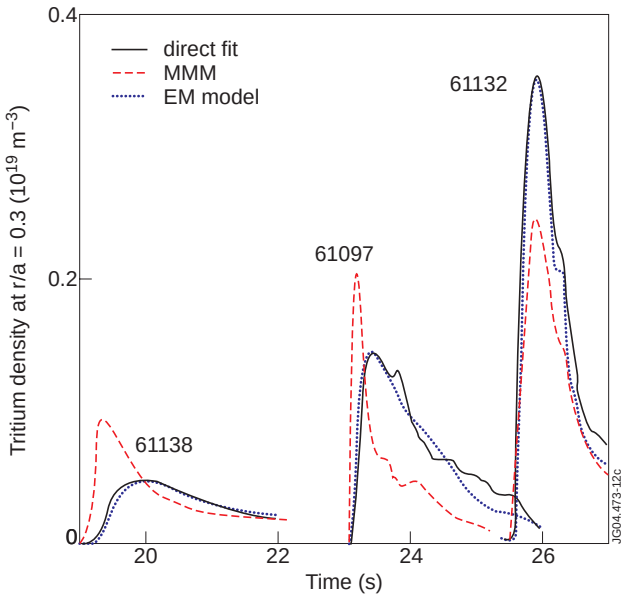

Figure 11: Evolution of T density (r/a = 0.3) for three discharges using the fitting method of section 2 (solid black), MMM model (dotted red) and an EM model [11] (dashed blue) A time shift of 3s is used for discharge 61132.

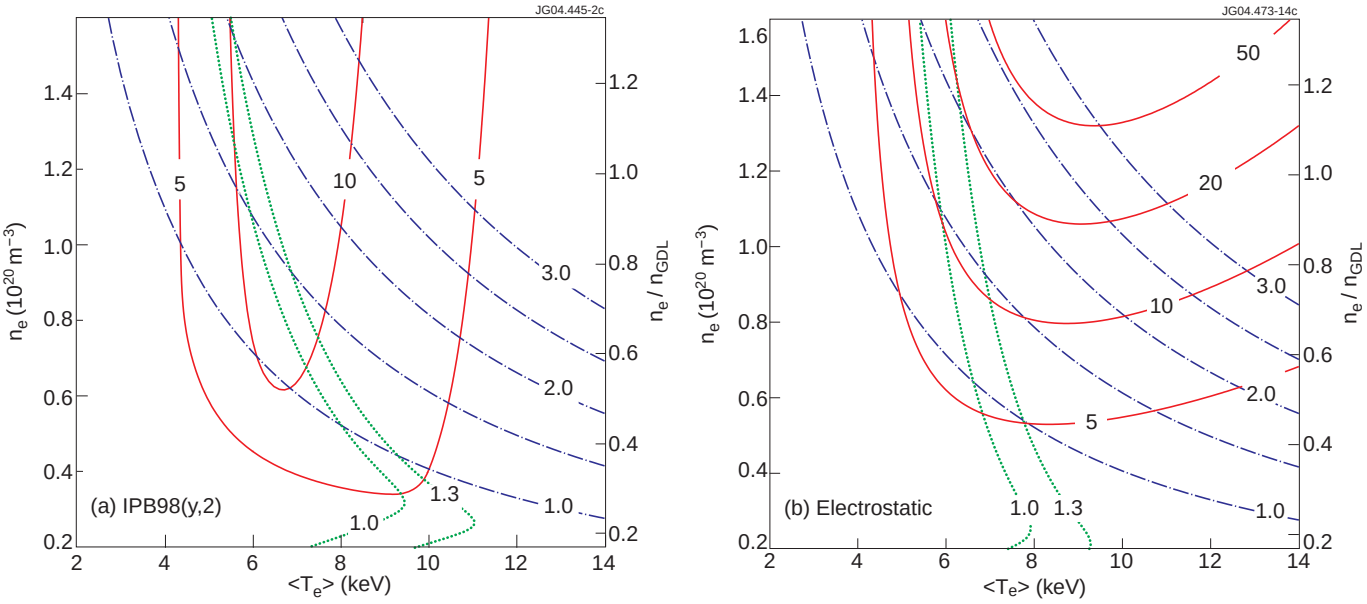

Figure 12: POPCON plots of the ITER operation space in volume averaged density and temperature showing contours of fusion gain Q (red solid lines), normalised…β (blue dashed and dotted line), and power relative to the L-H threshold (green dotted lines). Energy confinement is assumed to go as (a) IPB98(y,2), equation (1a), and (b) as in the electrostatic scaling of equation 7.